Journal of Catalysis **194,** 431–444 (2000)
doi:10.1006/jcat.2000.2938, available online at http://www.idealibrary.com on IDEAL®

Thermolytic Molecular Precursor Route to Active and Selective Vanadia–Zirconia Catalysts for the Oxidative Dehydrogenation of Propane

Jonathan L. Male,*,‡ Heiko G. Niessen,† Alexis T. Bell,†,‡,[1] and T. Don Tilley*,‡,[1]

*Department of Chemistry and †Department of Chemical Engineering, University of California, Berkeley, Berkeley, California 94720-1460; and ‡Chemical Sciences Division, Lawrence Berkeley National Laboratory, 1 Cyclotron Road, Berkeley, California 94720

Received March 20, 2000; accepted May 29, 2000

The thermolytic molecular precursor route was employed in attempts to obtain highly dispersed and structurally well-defined vanadia–zirconia catalysts for the oxidative dehydrogenation of propane. The vanadia–zirconia materials were prepared by cothermolysis of $OV(O^tBu)_3$ and $Zr(OCMe_2Et)_4$ in a nonpolar solvent, at relatively low temperatures. Prior to calcination, these materials have relatively high surface areas, are amorphous, and appear to be highly dispersed. After calcination to 773 K, nanocrystalline zirconia and various VO_x species, which appear to be dispersed on the zirconia surface, can be observed by PXRD and Raman, DR-UV-vis, and ^{51}V NMR spectroscopies. Higher vanadia loadings and/or an increased calcination temperature (823 K) resulted in formation of ZrV_2O_7 (as demonstrated by Raman, DR-UV-vis, and ^{51}V NMR spectroscopies). In general, the VO_x/ZrO_2 materials obtained from the molecular precursor method possess a greater surface area and exhibit a higher dispersion of VO_x species than materials of the same composition prepared by conventional impregnation methods. For catalysts derived from the alkoxides, the maximum rate for propane oxidative dehydrogenation is more than double that observed for VO_x/ZrO_2 materials prepared by impregnation, under similar conditions. Likewise, higher selectivities to propene (by more than 15%) were observed with materials derived from the alkoxides. However, analysis of the rate data for the new catalysts revealed that the active sites were also more active in catalyzing the secondary oxidation of propene. As a result of this, the ratio of secondary combustion to oxidative dehydrogenation rate constants (k_3/k_1) was similar for materials prepared by either wet impregnation or thermolysis of molecular precursors. © 2000 Academic Press

Key Words: **molecular precursors; alkoxides; vanadia; zirconia; oxidative dehydrogenation.**

INTRODUCTION

The efficient conversion of alkanes to alkenes, which serve as key intermediates to vital products in the chemical industry, is a highly desired goal (1–3).[2] There are several processes currently available for the catalytic dehydrogenation of alkanes, but these are based on an endothermic reaction (2, 4). Thus, these reactions must to be carried out at higher temperatures which can reduce selectivity (via hydrocarbon cracking), are energy demanding, and suffer from deactivation of the catalysts by coking (2, 4). The oxidative dehydrogenation (ODH) of alkanes offers advantages over the direct dehydrogenation process, since it is exothermic and therefore requires lower temperatures. However, the ODH of alkanes requires a selective catalyst to inhibit further oxidation of the desired alkene (2, 4). An example of the commercial use of this chemistry is the conversion of *n*-butane to maleic anhydride (2).

Of the numerous materials investigated as catalysts for the ODH of alkanes, a significant fraction employ vanadium, which offers relatively high catalytic activities and selectivities for production of the alkene (2, 4). In many studies of such catalysts, tetrahedral V^{5+} species have been proposed as the active sites (2, 4).

In published research on the ODH of alkanes with vanadia catalysts, various supports (4) have been employed, including magnesia (5), titania (6), alumina (5, 6), silica (6), and zirconia (6–8). Recent work with zirconia indicates that it is one of the better supports for vanadia in the ODH of hydrocarbons, since it gives high vanadia dispersions and is thermally stable and chemically inert (4, 6, 9–11). Furthermore, it has been shown that zirconia-supported vanadium oxide is more active than vanadia supported on niobia, alumina, and silica, using the oxidation of methanol as a probe reaction (12). This trend has also been shown to apply more generally to other oxidation reactions (13). There have been studies of vanadia–zirconia catalysts in selective oxidations of Z-but-2-ene (14), toluene (13, 15, 16), methanol (12), and propane (6–8).

A challenging aspect of the synthesis of vanadia-supported catalysts is the development of methods for the optimal dispersion of vanadium on the support, particularly at high loadings of vanadium. Such dispersions can be difficult to achieve by traditional wet impregnation methods,

[1] To whom correspondence should be addressed. E-mail: tdtilley@socrates.berkeley.edu; bell@cchem.berkeley.edu.

[2] North American capacities for ethene and propene were projected to be 7.1×10^{10} and 4.0×10^{10} lb, respectively, for 1999. See (1).

0021-9517/00 $35.00
Copyright © 2000 by Academic Press
All rights of reproduction in any form reserved.

because crystalline V_2O_5 domains tend to form under aqueous conditions (17, 18). We have developed an alternative, nonaqueous approach to the preparation of mixed-element oxides, which appears to allow a greater level of molecular-level control over the resulting structure. This approach, which we refer to as the *thermolytic molecular precursor method*, has been used to obtain highly dispersed mixed-element oxide materials (19–27). An example of this approach is given by the low-temperature thermolysis of group 4 tri(alkoxy)siloxy complexes $M[OSi(O^tBu)_3]_4$ (M = Ti, Zr, Hf), which convert readily to $MO_2 \bullet 4SiO_2$ materials with very high surface areas, at low temperatures (410–498 K) (21, 22). In addition, we have prepared $OV[OSi(O^tBu)_3]_3$ as a molecular precursor to catalytic materials and a model complex for isolated pseudotetrahedral vanadia on a silica surface (23, 24). More recently, we have found that this approach can be extended to combinations of alkoxide derivatives such that more complex stoichiometries are accessible (23).

In a previous report, we showed that the cothermolysis of $OV[OSi(O^tBu)_3]_3$ and $Zr[OCMe_2Et]_4$ produced vanadia–silica–zirconia materials that are superior to similar materials prepared by traditional wet impregnation methods with respect to surface area and catalytic performance in the ODH of propane (7, 23). To characterize the role of silica on the surface area and catalytic properties of the ZrO_2–SiO_2–V_2O_5 materials, we carried out the investigations described here, on the use of the thermolytic molecular precursor route to vanadia–zirconia catalysts.

Recent work with vanadia–zirconia catalysts prepared by the incipient wetness method provides an excellent series of materials with which to compare vanadia–zirconia catalysts prepared by the cothermolysis of alkoxides (6, 7). Hence vanadia–zirconia materials prepared from $OV(O^tBu)_3$ and $Zr[OCMe_2Et]_4$ have been thoroughly characterized and studied as ODH catalysts. In this contribution, we compare the performance of these catalysts with catalysts of the same composition but prepared by more traditional methods (6–8). We have found that catalysts obtained from molecular precursors possess a higher surface area and a greater dispersion of vanadia, and they give better intrinsic selectivities and activities for the conversion of propane to propene.

EXPERIMENTAL

Inside an inert atmosphere dry box, a thick-walled glass ampoule (100 mL) was charged with $Zr[OCMe_2Et]_4$ (Gelest, $5.0–6.2 \times 10^{-3}$ mol), $OV(O^tBu)_3$ ($4.4–20.0 \times 10^{-4}$ mol), and 8 mL of *n*-octane such that a constant total concentration of alkoxides (0.88 M) was maintained. The solution was degassed and the ampoule was flame-sealed under vacuum. The tube and its contents were placed in an oven at 458 K. Heating was maintained until a gel or polymeric oxide solid was observed, and then heating was continued for an additional 24 h to ensure complete conversion. The tube and its contents were allowed to cool; then the tube was opened and the solvent was allowed to slowly evaporate over 5 days under ambient conditions. The resultant solid material was further dried under a dynamic vacuum for $\geq$12 h and then heat-treated under dry air at either 773 or 823 K (typical heating regime: 3 K/min to 823 K, hold at 823 K for 3 h, cool at 10 K/min to room temperature). This typically resulted in 0.84 g of V_2O_5/ZrO_2 materials (98% yield assuming complete conversion to V_2O_5/ZrO_2), with 5, 10, 14, 18, and 23 wt% V_2O_5 ($5VO_x/ZrO_2$, $10VO_x/ZrO_2$, $14VO_x/ZrO_2$, $18VO_x/ZrO_2$, and $23VO_x/ZrO_2$, respectively).

Surface areas were measured by N_2 physisorption at 77 K (after outgassing freshly calcined samples under vacuum for $\geq$2 h at 393 K) using a Quantasorb surface area analyzer (Quantachrome Corporation) and standard multipoint Brunauer–Emmett–Teller (BET) analyses (5 points at P/P_0 values 0.1, 0.15, 0.2, 0.25, and 0.3; total pore volumes were determined at a P/P_0 value of 0.99). The average pore size and the distribution of pore radii were determined using the Barrett–Joyner–Halenda (BJH) method from desorption curves.

The TEM micrographs were obtained on a JEOL 100CX microscope at 80 kV operating in bright field mode. The samples were prepared by depositing a toluene suspension of the finely ground powders (ca. 1 wt%) onto carbon-coated copper grids (400 mesh, Ted Pella Inc.) that had previously been treated with an argon glow discharge.

Powder X-ray diffraction patterns were obtained at ambient temperature using Cu $K\alpha$ radiation and a Siemens D5000 diffractometer. A small amount of finely divided catalyst was sprinkled onto an irregular film of Vaseline on a mounted borosilicate disk, which was then loaded into the diffractometer. The diffraction patterns were corrected for any borosilicate background and the $K\alpha_2$ lines were removed. Raman spectra were obtained using a Hololab 5000 Raman research spectrophotometer (Kaiser Optical Systems, Inc.) with a 532-nm solid-state laser (Coherent Laser Group), a thermoelectrically cooled CCD detector (Princeton Instruments, Inc.), and finely divided solid samples sealed in glass capillaries.

Diffuse reflectance UV-vis (DR-UV-vis) spectra were obtained with a Varian–Cary 4 spectrophotometer equipped with a Harrick diffuse-reflectance attachment, using MgO as a reference. Vanadia/zirconia materials were placed in the Harrick diffuse-reflectance pod equipped with a heater, a water-cooling system, a thermocouple, and a gas flow system. The materials were dehydrated at 723 K for 1 h, then cooled to room temperature under dry air before the spectra were obtained.

Solid-state ^{51}V NMR spectra were acquired on a home-built spectrometer with a field strength of 9.4 T (400 MHz

resonance frequency for ^1H). The static wide-line spectra were obtained with a single pulse sequence (pulse angle 1 μs, delay 500 ms, spectral width of 500 kHz, line broadening 500 Hz, no proton decoupling, typically 12,000 scans). Static ^{51}V NMR spectra were obtained using freshly calcined samples sealed in 20–30 mm long, 5 mm diameter NMR tubes under vacuum. A vacuum-sealed sample of neat $VOCl_3$ was used as an external zero point reference ($RF = 105.213$ MHz).

Rates of reactions and selectivities for the oxidative dehydrogenation of propane were measured in a fixed-bed quartz reactor with a medium frit using 4.0–50.0 mg of catalyst and quartz powder (0.50 g, particle size 0.246–0.495 mm). The gas stream consisted of helium (typically 200 $cm^3\ min^{-1}$), propane (25 $cm^3\ min^{-1}$), nitrogen (2 $cm^3\ min^{-1}$), and oxygen (9 $cm^3\ min^{-1}$). The gaseous reactants and products were analyzed on-line using a Hewlett–Packard 6890 gas chromatograph equipped with both a capillary column (HP-1) and a packed column (HAYESEP-Q). Only C_3H_6, CO, CO_2, and H_2O were detected as reaction products. Propane and oxygen conversions were varied by changing the total flow rate (50–236 $cm^3\ min^{-1}$) and the temperature of the reaction (606, 673, and 723 K). Typical propane conversions ranged from 0.1–5.0% with oxygen consumptions of 0.1–25%.

RESULTS

Catalyst Synthesis

The alkoxides $OV(O^tBu)_3$ and $Zr[OCMe_2Et]_4$ were chosen as the starting materials for synthesizing vanadia–zirconia xerogels (23). In a sealed capillary, $OV(O^tBu_3)_3$ melts at 319–321 K and decomposes at about 446 K. A thermal gravimetric analysis of this compound revealed a precipitous weight loss, characterized by an onset temperature of 405 K, which was complete by about 458 K. Under the typical conditions used for alkoxide thermolysis (sealed ampoule, 8 mL *n*-octane), $Zr[OCMe_2Et]_4$ does not thermally decompose until 523 K (over 24 h). The vanadia–zirconia materials described here were obtained by heating solutions of the alkoxides at 458 K. This suggests that the vanadium alkoxide decomposes first, and the resulting decomposition products then catalyze the decomposition of $Zr[OCMe_2Et]_4$. After thermolysis and slow drying of the materials in air, beige-colored solids were obtained. Calcination (773–823 K) under dry air gave visually homogeneous, pale yellow to yellow-green (depending on the vanadium loading) powders.

Vanadia–zirconia materials obtained by the wet impregnation of zirconia with ammonium metavanadate (7) were calcined at 673, 773, and 873 K under dry air, and the catalytic performances were examined at 606 and 673 K. The vanadia–zirconia materials obtained via the thermolytic molecular precursor route were calcined at both 773 and 823 K. The use of two calcination temperatures also allowed investigation of the effect of sintering on the reactivities, dispersions, and structures of the vanadia–zirconia catalysts.

Characterization of Vanadia–Zirconia Materials

The surface areas, total pore volumes, and average pore radii of the vanadia–zirconia materials before and after calcination in air are shown in Table 1, and the surface areas are compared to those for materials obtained by the wet

TABLE 1

Vanadium Content, Surface Area, and Calculated VO_x Surface Density for VO_x/ZrO_2 Materials

Calcination temperature (K)	Sample	wt% V_2O_5	BET surface area (S_{BET}) ($m^2\ g^{-1}$)[a]	Apparent surface density ($VO_x\ nm^{-2}$)[b]	Total pore volume ($cm^3\ g^{-1}$)	Average pore radius (Å)[c]	Average particle diameter (nm)[d]
773	$5VO_x/ZrO_2$	5	205 (541)	1.88	0.131 (0.421)	13.6	6
773	$10VO_x/ZrO_2$	10	294 (585)	2.25	0.225 (0.486)	16.2	6
773	$14VO_x/ZrO_2$	14	313 (662)	2.96	0.206 (0.529)	13.5	3
773	$18VO_x/ZrO_2$	18	284 (611)	4.20	0.192 (0.443)	13.9	4
773	$23VO_x/ZrO_2$	23	23.9 (476)	68.9	0.0488 (0.342)	40.9	16 (27)[e]
823	$5VO_x/ZrO_2$	5	164 (578)	2.02	0.110 (0.479)	15.2	7
823	$10VO_x/ZrO_2$	10	164 (674)	4.04	0.132 (0.588)	17.2	7
823	$14VO_x/ZrO_2$	14	143 (606)	6.50	0.148 (0.478)	22.1	7
823	$18VO_x/ZrO_2$	18	163 (607)	7.31	0.180 (0.443)	21.1	8
823	$23VO_x/ZrO_2$	23	28.5 (549)	56.2	0.124 (0.405)	87.4	13 (30)[e]

[a] The values in parentheses are for the material prior to calcination.
[b] The apparent surface density was calculated assuming all of the VO_x present is on the surface.
[c] Average pore radius is obtained from (2 × total pore volume)/surface area.
[d] Average diameter particle size of *t*-ZrO_2 determined from the powder X-ray diffraction data and the Scherrer equation.
[e] Average particle diameter for ZrV_2O_7 (given in parentheses) determined from the powder X-ray diffraction data and the Scherrer equation.

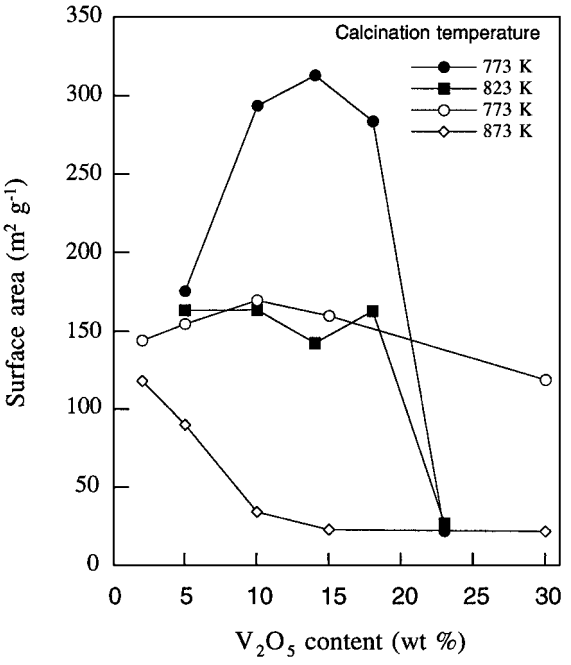

FIG. 1. Surface areas of VO_x/ZrO_2 catalysts prepared by thermolysis (filled symbols) and impregnation (open symbols) and subsequently calcined at 773, 823, and 873 K.

impregnation method (6, 7) in Fig. 1. The materials calcined at 773 K exhibit a maximum surface area for vanadia contents between 10 and 18 wt% V_2O_5, and $23VO_x/ZrO_2$ displays a highly reduced surface area, perhaps due to the crystallization of V_2O_5 or ZrV_2O_7 (*vide infra*). The adsorption/desorption isotherms for the 5–18 wt% V_2O_5/ZrO_2 materials (type I with a type H4 hysteresis loop (28)), and the corresponding average pore radius of <20 Å, describe these materials as being primarily microporous. The $23VO_x/ZrO_2$ material exhibited an approximately type III adsorption/desorption isotherm, with a type H4 hysteresis loop, and consistent with the presence of larger primary particles, this material exhibits an average pore radius of 41 Å (7, 9).

After calcination at 823 K, most of the V_2O_5/ZrO_2 materials exhibit a smaller surface area (by ca. 50%) relative to analogous materials heated at 773 K (Fig. 1). This is presumably due to the greater sintering of particles at this higher temperature. The surface areas for the 5–18 wt% V_2O_5 materials are relatively constant in value. The average pore radii of the materials with lower V_2O_5 loadings (5 and 10 wt%) are similar to those for materials calcined at 773 K and are predominantly microporous.

The crystallization behavior for the vanadia–zirconia materials was investigated by monitoring powder X-ray diffraction (XRD) patterns as a function of calcination temperature and vanadium loading. As expected, all the uncalcined materials were amorphous. Figures 2a and 2b present XRD patterns for all the materials studied, calcined at 773 and 823 K, respectively. For the lower vanadium loadings (5 and 10 wt%) calcined at 773 K (Fig. 2a), only diffraction peaks for metastable tetragonal zirconia (*t*-ZrO_2) (7, 9, 29) were observed. The diffraction patterns for the 14 and 18 wt% V_2O_5 samples are virtually featureless, with only low-intensity, broad peaks due to *t*-ZrO_2 being evident. This suggests the presence of a predominantly amorphous phase or a material possessing very small crystalline domains. The X- ray diffraction pattern for $23VO_x/ZrO_2$ exhibits intense peaks for *t*-ZrO_2 and minor peaks for monoclinic zirconia (*m*-ZrO_2), zirconium vanadate, and possibly V_2O_5 (7, 9, 29). For the V_2O_5/ZrO_2 materials calcined at 823 K (Fig. 2b)

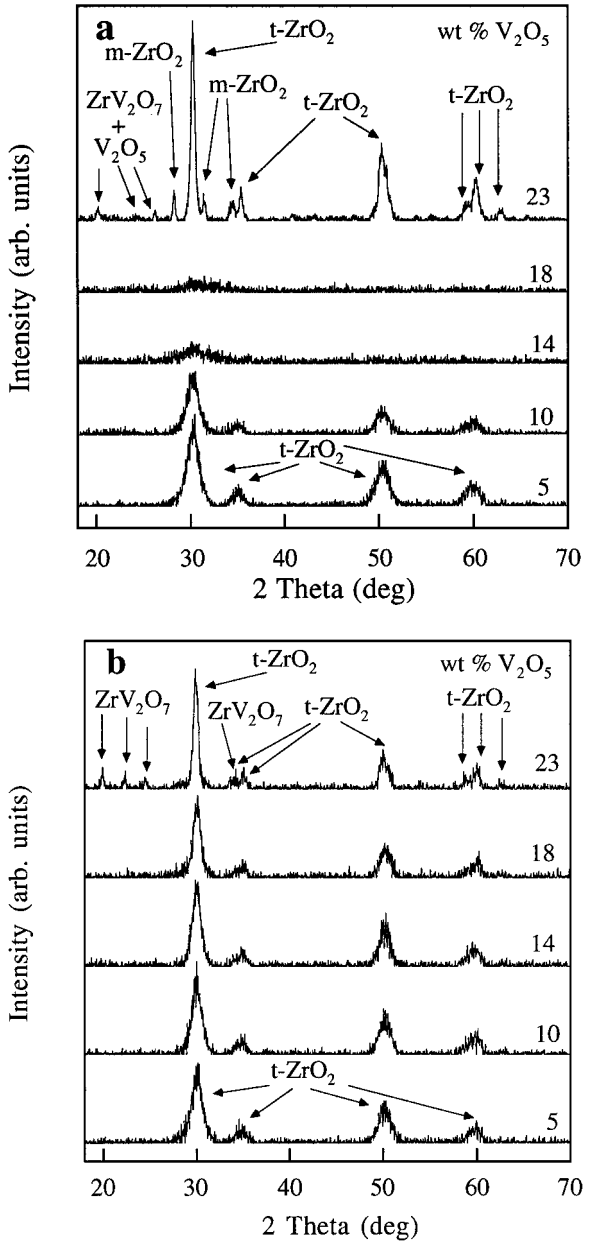

FIG. 2. Powder X-ray diffraction patterns of VO_x/ZrO_2 catalysts calcined at (a) 773 and (b) 823 K.

there is very little difference in the X-ray diffraction patterns for samples with 5–18 wt% V_2O_5 loadings, in that the sole species observed is *t*-ZrO_2 (7, 9, 29). For 23VO_x/ZrO_2 the major crystalline species present is *t*-ZrO_2, with minor amounts of zirconium vanadate (7, 9, 29).

Application of the Scherrer equation (30) to the XRD data indicates that there is not a significant change in crystallite size with calcination temperature (see Table 1). Thus, whereas the samples calcined at 773 K possess *t*-ZrO_2 crystallites with average diameters of 6–7 nm for the the 5–10 wt% V_2O_5/ZrO_2 samples, 3–4 nm for the 14–18 wt% V_2O_5/ZrO_2 samples, and 16 nm for 23VO_x/ZrO_2, the samples calcined to 823 K exhibit average diameters of 5–8 nm (5–18 wt% V_2O_5/ZrO_2) and 13 nm (23VO_x/ZrO_2). In addition, the 23VO_x/ZrO_2 materials calcined to 773 and 823 K possess crystallites of ZrV_2O_7 with average sizes of 27 and 30 nm, respectively.

To further investigate the morphology of these materials, they were examined by transmission electron microscopy (TEM). The images obtained revealed little difference between samples calcined at the two temperatures, with 5–14 wt% V_2O_5 loadings. As shown in Fig. 3, which provides a TEM micrograph of 10VO_x/ZrO_2 calcined at 823 K, the materials appear to be composed of aggregates of small particles with diameters of ca. 10 nm.

The Raman spectra of the VO_x/ZrO_2 materials calcined at 773 and 823 K are shown in Figs. 4a and 4b, respectively. With low vanadia loading (5 wt%), calcination to 773 K results in crystallization of *t*-ZrO_2 (272, 464, 639 cm^{-1}) and possibly some *m*-ZrO_2 (312 cm^{-1}) (6, 16, 31, 32). A broad band at 847 cm^{-1} is assigned to both V–O–Zr and polymeric

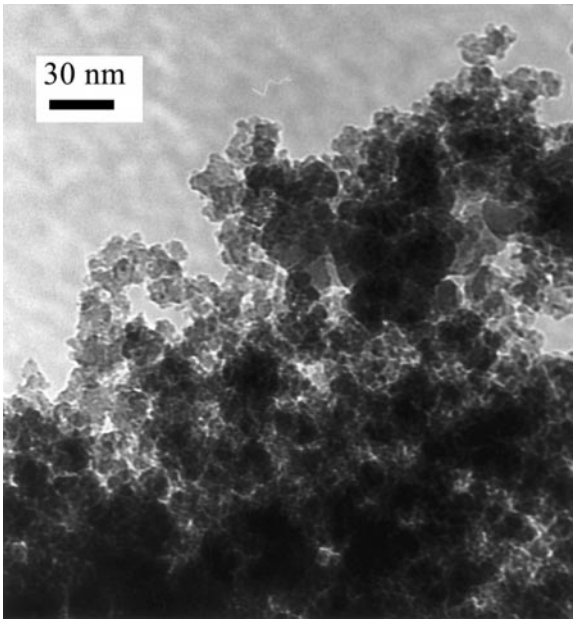

FIG. 3. Transmission electron micrograph of 10VO_x/ZrO_2 calcined at 823 K.

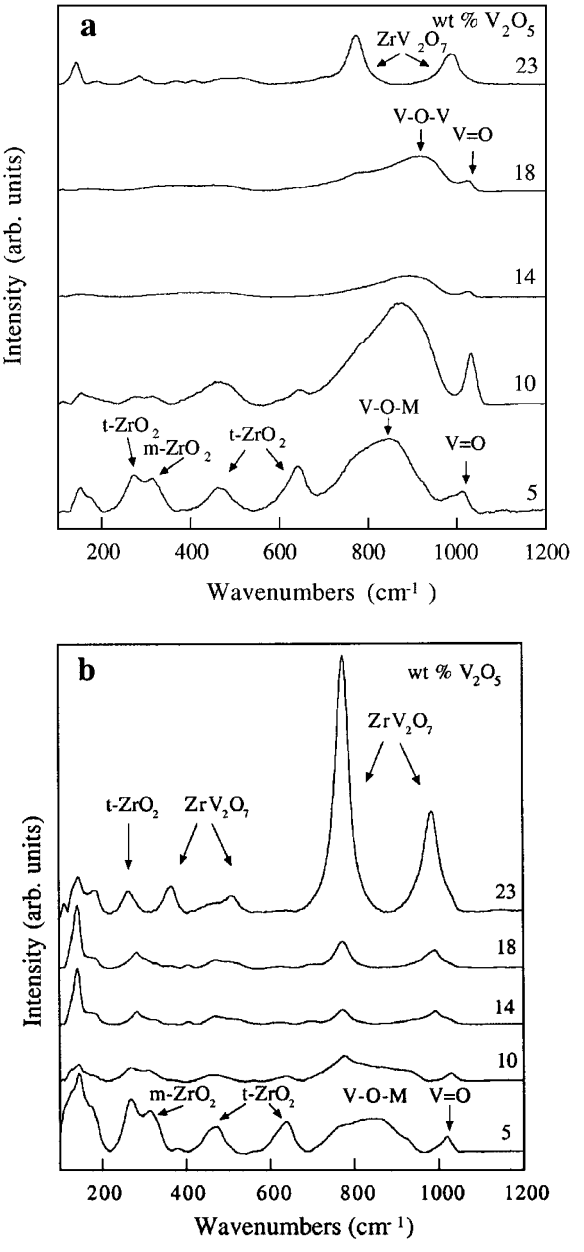

FIG. 4. Raman spectra of VO_x/ZrO_2 catalysts calcined at (a) 773 and (b) 823 K.

VO_x (V–O–V) species, and the sharp band at 1011 cm^{-1} is assigned to the V=O oscillation of an isolated VO_x species on zirconia (6, 31). The Raman spectrum of 10VO_x/ZrO_2 (calcined to 773 K) exhibits similar bands for zirconia, but with reduced intensities, and shifted bands assigned to VO_x (874 and 1030 cm^{-1}) are more intense, as might be expected for a higher vanadium loading (6, 16, 31, 33). The observed shift in the energy of the band attributed to V–O–M has been associated with oligomerization of the VO_x species (33–36). Raman spectra for 14VO_x/ZrO_2 and 18VO_x/ZrO_2 exhibit weak, broad bands assigned to *t*-ZrO_2 and the aforementioned bands associated with VO_x (891 and 1024 cm^{-1}

for $14VO_x/ZrO_2$; 913 and 1020 cm^{-1} for $18VO_x/ZrO_2$) (6, 31, 32). Thus, the shift in V–O–M vibrations due to VO_x polymerization continues further as the vanadium loading increases. An additional band at 770 cm^{-1}, observed as a shoulder in $18VO_x/ZrO_2$, is attributed to ZrV_2O_7 (6, 16, 37). The Raman spectrum of $23VO_x/ZrO_2$ exhibits bands at 367, 509 (shoulder), 770, and 985 cm^{-1} assigned to ZrV_2O_7 (16, 37), and a broad band at 466 cm^{-1} is attributed to *t*-ZrO_2 (6, 31, 32). In addition, weak bands at 283 and 405 cm^{-1} are tentatively assigned to trace amounts of V_2O_5 (6). Note that the Raman assignments are consistent with results from the powder X-ray diffraction patterns for these materials, except that *m*-ZrO_2 was not observed in the $23VO_x/ZrO_2$ sample calcined to 773 K. As has been previously observed, Raman bands due to *m*-ZrO_2 can be very weak or unobserved, even when powder X-ray diffraction patterns demonstrate that the monoclinic form is present (31).

For $5VO_x/ZrO_2$ calcined at 823 K, the Raman spectrum (Fig. 4b) contains bands assigned to *t*-ZrO_2 (268, 461, and 637 cm^{-1}), possibly some *m*-ZrO_2 (308 cm^{-1}), polymeric V–O–V or V–O–Zr (broad asymmetric band at 857 cm^{-1}), and isolated vanadyl (V=O, 1017 cm^{-1}). While $10VO_x/ZrO_2$ (calcined at 823 K) exhibits virtually identical bands (but with reduced intensities), a broad asymmetric resonance at about 900 cm^{-1} indicates the presence of oligomeric VO_x. Note that the V=O stretch in this sample has shifted to 1026 cm^{-1}. In addition, there is a weak band at 774 cm^{-1} assigned to low levels of ZrV_2O_7. Thus, the Raman spectrum of this material is very similar to those observed for $14VO_x/ZrO_2$ and $18VO_x/ZrO_2$ calcined at 773 K. The 14 and 18 wt% V_2O_5/ZrO_2 samples calcined at 823 K have virtually identical spectra, with $18VO_x/ZrO_2$ exhibiting more intense bands, except that the broad feature corresponding to oligomeric VO_x is absent in these spectra. Strong bands at 770 and 991 cm^{-1} in these spectra are assigned to ZrV_2O_7 (16), and bands due to V_2O_5 (283, 406, and 693 cm^{-1}) and *t*-ZrO_2 (468 cm^{-1}) are also observed (6, 16, 32). The Raman spectrum of $23VO_x/ZrO_2$ contains bands for both *t*-ZrO_2 and ZrV_2O_7.

Figures 5a and 5b present diffuse reflectance UV-vis (DR-UV-vis) spectra for the vanadia–zirconia materials calcined at 773 K and 823 K, respectively. With the vanadia–zirconia materials calcined at 773 K a gradual shift of the absorption edge energies to lower values with increasing V_2O_5 loading was observed (Fig. 5a). The absorption edge energies lie within the limits defined by those for the model pseudotetrahedral compound $OV[OSi(O^tBu)_3]_3$ (3.95 eV) (24) and V_2O_5 (possessing a distorted octahedral environment; 2.48 eV).[3] This trend indicates a progression from

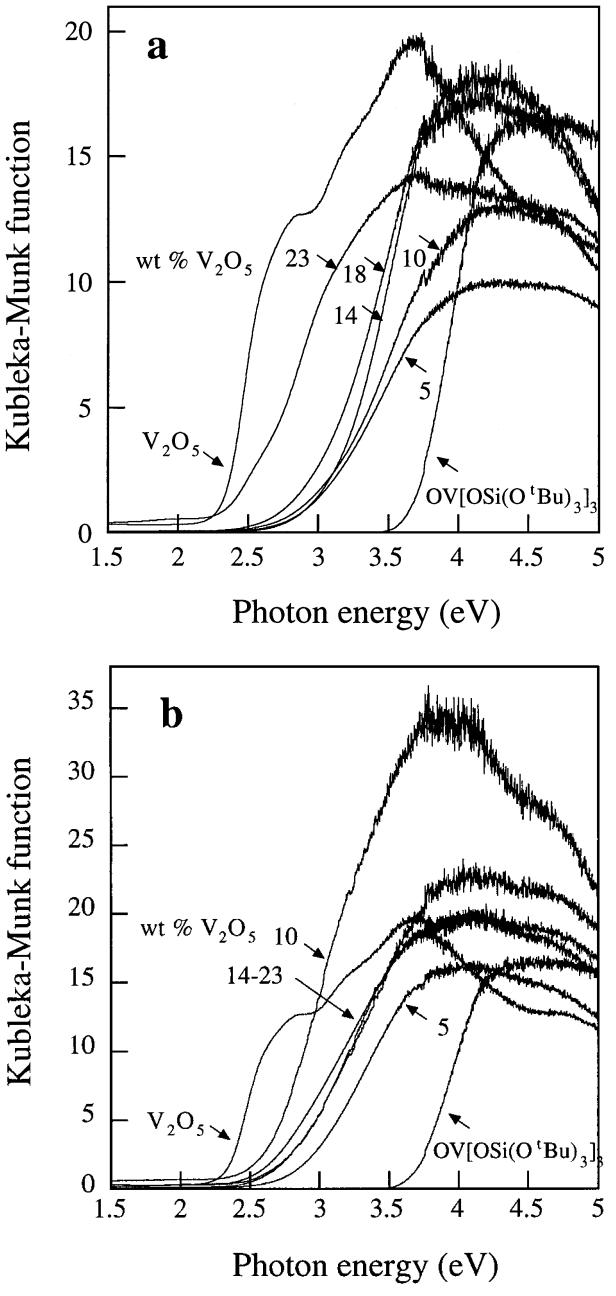

FIG. 5. DR-UV-vis spectra of VO_x/ZrO_2 catalysts calcined at (a) 773 K and (b) 823 K together with reference materials (V_2O_5, $OV[OSi(O^tBu)_3]_3$).

isolated pseudotetrahedral VO_x, to oligomeric VO_x species, to V_2O_5 (6, 7), and is consistent with that deduced from Raman spectroscopy. By contrast, the DR-UV-vis spectra of the vanadia–zirconia materials calcined at 823 K (Fig. 5b) do not display a gradual transition to lower absorption edge energies upon increasing V_2O_5 loadings. The absorption edge energy for $5VO_x/ZrO_2$ resembles that expected for isolated pseudotetrahedral VO_x species. The lower energy absorption edge for $10VO_x/ZrO_2$ is consistent with oligomeric

[3] The values for UV-vis absorption energies given in parentheses are derived from the first inflexion point. The values using Tauc's law for indirect and amorphous semiconductors would be 3.48 eV for $OV[OSi(O^tBu)_3]_3$ and 2.21 eV for V_2O_5 (6).

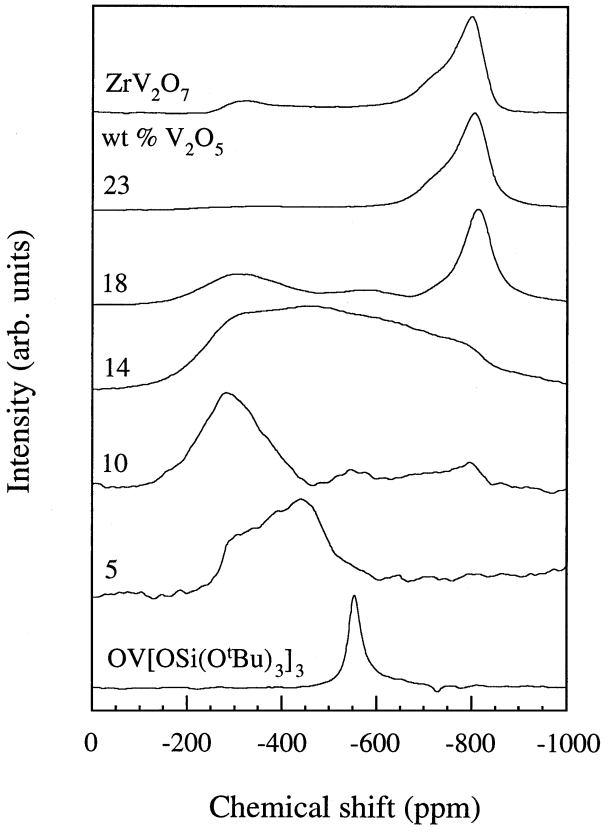

FIG. 6. Solid-state ^{51}V NMR spectra of VO_x/ZrO_2 catalysts calcined at 823 K and of reference materials (ZrV_2O_7, $OV[OSi(O^tBu)_3]_3$).

VO_x whereas the samples with 14–23 wt% loadings display an absorption edge energy corresponding to a pseudotetrahedral environment. This difference in behavior for samples calcined at 773 and 823 K is attributed to the formation of significant amounts of ZrV_2O_7 (two tetrahedral vanadium centers with one bridging oxygen (38)) with calcination to the higher temperature.

To further explore the structures of the vanadia–zirconia materials calcined at 823 K, ^{51}V solid-state NMR spectra were obtained and compared to spectra for $OV[OSi(O^tBu)_3]_3$, ZrV_2O_7, and V_2O_5 (39–41) (Fig. 6). The compound $OV[OSi(O^tBu)_3]_3$, which serves as a model for isolated pseudotetrahedral vanadium oxide centers (24), exhibits a strong resonance at −552 ppm (FWHH = 4280 Hz) associated with a pair of quadrupolar satellite transitions (−3/2 to −1/2, 1/2 to 3/2) at ±70 kHz. The tetrahedral vanadium in ZrV_2O_7 exhibits an asymmetric resonance with the most intense line-shape component at −800 ppm (9, 38). The distorted octahedral vanadium environment of V_2O_5 exhibits a major resonance at ca. −320 ppm (9, 39–41).

As seen in Fig. 6, the material with the lowest vanadium loading (5 wt%) exhibits an anisotropic resonance with two primary components (major, −450 ppm; minor, −280 ppm), while $10VO_x/ZrO_2$ exhibits three resonances (major, −280 ppm; minor, −800, −450 ppm). The resonance at −450 ppm is assigned to a pseudotetrahedral $O{=}VO_3$ species, while the resonance at −280 ppm may be attributed to vanadium centers with a higher coordination number (9, 39–41). The small resonance at −800 ppm in $10VO_x/ZrO_2$ indicates the presence of a small amount of ZrV_2O_7 (9). Broad sets of resonances in $14VO_x/ZrO_2$, which are more defined in $18VO_x/ZrO_2$, appear to represent pseudotetrahedral $O{=}VO_3$, vanadium with a higher coordination number, and ZrV_2O_7. As expected from the results presented above, the higher vanadium loading results in greater conversion to ZrV_2O_7. For $23VO_x/ZrO_2$, calcination at 823 K appears to result in almost complete conversion to ZrV_2O_7.

Catalyst Characterization

Representative data for the conversion of propane to propene, CO, and CO_2 (as catalyzed by $14VO_x/ZrO_2$ calcined at 773 K) at a reaction temperature of 606 K is given in Fig. 7 as a plot of rate of production of products and propene selectivity versus reciprocal flow rate (normalized for mass). As previously observed, with increasing catalyst bed residence time the conversion of propane and propene to CO_x increases (6, 7). Neither ZrO_2 (6) nor the quartz chips used to dilute the catalyst show any catalytic activity at temperatures between 606 and 773 K. In order to determine the intrinsic activity and selectivity of the catalysts at zero propane and oxygen conversions, values for both characteristics were linearly extrapolated to zero residence time.

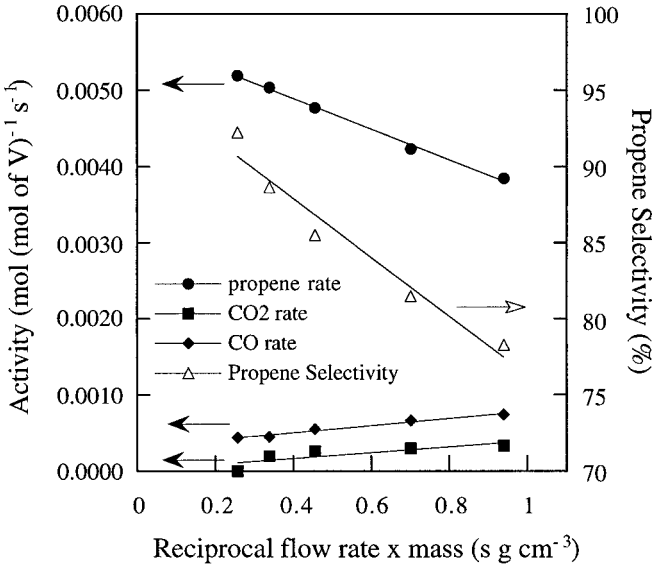

FIG. 7. Rates of C_3H_6, CO, and CO_2 formation and propene selectivity as functions of the reciprocal of the flow rate normalized for catalyst mass for $14VO_x/ZrO_2$ (calcined at 773 K). Reaction conditions: 606 K; initial total flow rate and composition, $C_3H_8/He/N_2/O_2$ 25/199/2/9 cm^3 min^{-1}; pressure, 1 atm; mass of catalyst, 0.0070 g.

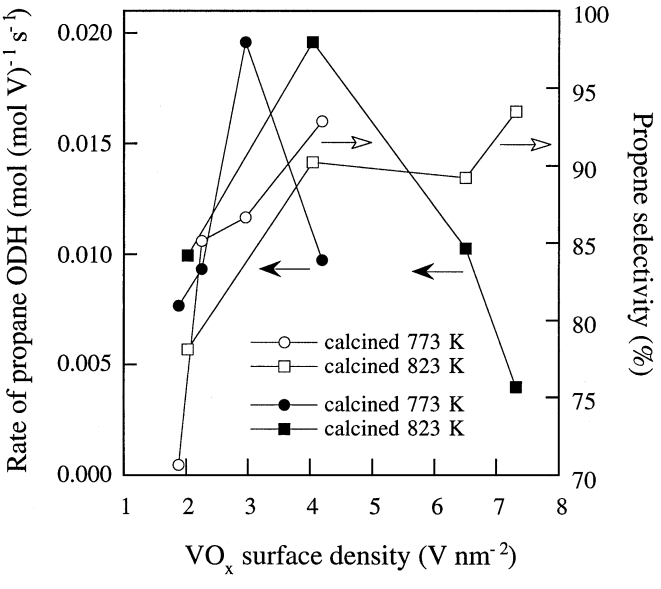

FIG. 8. Rate of propene production and propene selectivity as a function of apparent VO_x surface density for VO_x/ZrO_2 catalysts calcined at 773 and 823 K. Reaction conditions: 673 K; typical initial total flow rate and composition, $C_3H_8/He/N_2/O_2$ 25/199/2/9 cm^3 min^{-1}; pressure, 1 atm; mass of catalysts, 0.0047–0.0500 g.

Plots of the rate of propene production and propene selectivity (both at zero residence time) as a function of the apparent vanadium surface density are shown in Fig. 8 for vanadia–zirconia materials calcined at 773 and 823 K. The apparent surface density of VO_x is used as a variable (see Table 1), bearing in mind that some of the vanadium may be part of the bulk as a consequence of the preparation from alkoxide precursors. This concern is addressed more fully below. The intrinsic rate of propene production with respect to surface density of VO_x (Fig. 8 and Table 2) suggests that for materials calcined at 773 K the optimum loading is 14 wt% V_2O_5 (3 VO_x nm^{-2}), while for the materials calcined at 823 K the optimum is 10 wt% V_2O_5 (4 VO_x nm^{-2}). There is very little difference between the activities of the most active catalysts when the reaction temperatures are altered (606–723 K). The activities of $23VO_x/ZrO_2$ (calcined at 773 and 823 K) are significantly lower (see Table 2) than those of other samples, presumably due to the formation of either bulk V_2O_5 or ZrV_2O_7 and the consequent inaccessiblity of vanadium sites in these species.

Figure 8 also shows that the propene selectivity increases for both sets of materials up to a surface density value of ca. 3.5 VO_x nm^{-2}, after which the selectivity for propene is virtually constant at about 90% at a reaction temperature of 673 K. For $23VO_x/ZrO_2$ calcined at 773 and 823 K (not shown), the propene selectivities were 87 and 99% at surface densities of 69 and 56 VO_x nm^{-2}, respectively. Typically, as the reaction temperature was increased (606–723 K) the selectivity to propene was slightly reduced (see Table 3), but the onset of the plateau corresponding to maximum selectivity is always at ca. 3.5 VO_x nm^{-2}.

TABLE 2

Catalytic Activities for VO_x/ZrO_2 Materials

Catalyst	Activity[a] (606 K)		Activity[a] (673 K)		Activity[a] (723 K)	
	mmol g • h	mmol mol • s	mmol g • h	mmol mol • s	mmol g • h	mmol mol • s
$5VO_x/ZrO_2$[b]	4.3	2.2	15.2	7.7	19.2	9.7
$10VO_x/ZrO_2$[b]	10.8	2.7	36.9	9.3	70.7	17.9
$14VO_x/ZrO_2$[b]	31.5	5.7	109	19.6	181	32.8
$18VO_x/ZrO_2$[b]	22.8	3.2	69.4	9.7	162	22.8
$23VO_x/ZrO_2$[b]	1.6	0.17	5.5	0.60	13.7	1.5
$5VO_x/ZrO_2$	6.1	3.1	19.7	9.9	42.6	21.5
$10VO_x/ZrO_2$	21.3	5.4	77.5	19.6	172	43.4
$14VO_x/ZrO_2$	16.9	3.1	56.8	10.3	129	23.3
$18VO_x/ZrO_2$	9.0	1.3	28.2	4.0	67.3	9.5
$23VO_x/ZrO_2$	3.7	0.40	15.5	1.7	37.3	4.1

[a] Mass of catalysts range: 0.0047–0.0500 g. Typical initial flow rate and composition: $C_3H_8/He/N_2/O_2$ 25/199/2/9 cm^3 min^{-1}. Total pressure: 1 atm. Values given in the table were obtained by extrapolation to zero in plots of activity vs (1/flow rate) mass.

[b] The sample was calcined at 773 K. All other samples were calcined at 823 K.

The thermal stabilities of the most active vanadia–zirconia catalysts prepared from molecular precursors ($14VO_x/ZrO_2$ calcined at 773 K; $10VO_x/ZrO_2$ calcined at 823 K) were examined at 723 K with a total gas flow rate of 231 cm^3 min^{-1}. Both catalysts were found to be stable over 19 and 17.5 h, with rates for the production of propene of 32.2 ± 0.5 and 32.8 ± 0.6 mmol (mol of V)$^{-1}$ s^{-1}, respectively.

TABLE 3

Propene Selectivities for VO_x/ZrO_2 Materials

Catalyst	Propene selectivity (%)[a] (606 K)	Propene selectivity (%)[a] (673 K)	Propene selectivity (%)[a] (723 K)
$5VO_x/ZrO_2$[b]	70	71	56
$10VO_x/ZrO_2$[b]	91	85	65
$14VO_x/ZrO_2$[b]	96	87	85
$18VO_x/ZrO_2$[b]	98	93	90
$23VO_x/ZrO_2$[b]	100	87	90
$5VO_x/ZrO_2$	78	78	74
$10VO_x/ZrO_2$	88	90	84
$14VO_x/ZrO_2$	90	89	82
$18VO_x/ZrO_2$	94	93	83
$23VO_x/ZrO_2$	100	99	86

[a] Mass of catalysts range: 0.0047–0.0500 g. Typical initial flow rate and composition: $C_3H_8/He/N_2/O_2$ 25/199/2/9 cm^3 min^{-1}. Total pressure: 1 atm. Values given in the table were obtained by extrapolation to zero in plots of activity vs (1/flow rate) mass.

[b] The sample was calcined at 773 K. All other samples were calcined at 823 K.

DISCUSSION

Characterization of Vanadia–Zirconia Materials

BET surface analyses reveal interesting trends describing the effect of vanadium content and calcination temperature on the morphologies of the vanadia–zirconia materials prepared by the thermolytic molecular precursor route. As shown in Fig. 1 and Table 1, the lower calcination temperature results in higher surface areas and total pore volumes for most vanadia contents. This general trend might be expected to result from greater sintering at the higher temperature. However, interestingly, this effect is moderated by the presence of vanadia. At the lowest vanadia content (5 wt%), sintering appears to occur to similar extents irrespective of calcination temperature, to result in the same surface area. This is consistent with what might be expected for pure zirconia, which is a refractory material (9, 10). In fact, the XRD data show that the *t*-ZrO_2 particles which have crystallized by 773 K have not grown significantly in size after heating at 823 K (Table 1). As shown in Figure 2a, XRD data for samples calcined to the lower temperature (773 K) indicate that vanadia increasingly inhibits the crystallization of zirconia from 10–18 wt% V_2O_5 (9, 29, 42, 43). This is also consistent with the calculated *t*- ZrO_2 particle sizes given in Table 1, which indicate that calcination to the higher temperature leads to very little growth of the crystallites. Note that the behavior of the material with the largest vanadia content (23 wt%) does not follow the above trends. For $23VO_x/ZrO_2$, calcination to either temperature results in the same low surface area. In addition, the average diameters of the *t*-ZrO_2 crystallites in these samples are markedly larger (ca. 13–16 nm). The anomalous behavior for the $23VO_x/ZrO_2$ samples is explained by XRD, Raman, and ^{51}V NMR data, which reveal that significant quantities of ZrV_2O_7 are formed at this loading. Thus, it appears that in these samples the formation of relatively large ZrV_2O_7 particles (with average diameters of ca. 30 nm) removes vanadia domains from the system and results in a lower surface area and less inhibited growth of the *t*-ZrO_2 particles.

The crystallization behavior described above may be rationalized by a proposed sequence of events starting with the crystallization of nanosized domains of *t*-ZrO_2, the inhibition of which is consistent with an initial, intimate mixing of the vanadium and zirconium. As the crystallization of zirconia proceeds, the excluded vanadium species aggregate at the surface of the growing zirconia crystallites. Small vanadia aggregates on the surface of zirconia have little effect on the sintering behavior of the system, but larger vanadia loadings (10–18 wt%) result in coated particles for which further growth is inhibited (44–46). The lower (and relatively constant) surface areas observed for materials calcined at the higher temperature may be explained by the formation of ZrV_2O_7, which removes VO_x species from the system (*vide supra*). Thus, as the vanadia content is increased to 18%, calcination at 823 K leads to materials having surface areas close to that of $5VO_x/ZrO_2$.

A significant element of the model described above is the description of the primary particles in calcined samples possessing vanadia contents of $\leq$18% as small *t*-ZrO_2 crystallites coated with VO_x species. This view is supported by observed reductions in the intensities of Raman bands for zirconia with increasing vanadia content (Figs. 4a and 4b). Previously, this effect has been attributed to modulation of the back-scattered Raman signal for ZrO_2 by well-dispersed vanadium oxide on the surface of the material (16, 31, 37). At the higher vanadium loadings and higher temperature, where the vanadium is present mostly as ZrV_2O_7, the Raman signals for ZrO_2 are increased in intensity.

As has been observed in similar vanadia–zirconia systems (7, 9, 11, 31, 43) the presence of vanadia inhibits the formation of *m*-ZrO_2 (the thermodynamically more stable form at low temperatures) by stabilizing the nanoparticles of *t*-ZrO_2 which form kinetically. At both calcination temperatures, the 10–18 wt% V_2O_5 materials contain *t*-ZrO_2 and apparently no *m*-ZrO_2 (by XRD and Raman spectroscopy; Figs. 2a, 2b, 4a, and 4b) (29, 42). Consistently, with little vanadium present (5 wt%) the transformation to *m*-ZrO_2 is not inhibited, and at the highest vanadia loading (23%) the crystallization of ZrV_2O_7 consumes significant quantities of the vanadium present, such that the formation of *m*-ZrO_2 is again observed.

Consistent with the model presented above for rationalizing the crystallization behavior of the vanadia–zirconia systems under study, it is well known that vanadia disperses relatively well on zirconia particles (6, 9, 13, 33). At low loadings, the vanadium species in calcined vanadia–zirconia materials are present predominantly as isolated $O{=}VO_3$ species bound to the surface of zirconia (6, 7, 9, 33). These species can pack into a monolayer up to a surface density of 2.3 VO_x nm^{-2}, and further increases in VO_x concentration result in formation of a two-dimensional polyvanadate monolayer (up to a surface density of 7.5 VO_x nm^{-2} (7, 9)). As might be expected, the XRD patterns for the 5-$18VO_x/ZrO_2$ materials reveal no crystalline vanadium-containing species (Figs. 2a and 2b). This presumably means that the vanadium is present in an amorphous phase or in very small, ordered domains. The Raman spectra for the 5–$18VO_x/ZrO_2$ materials calcined to 773 K (Fig. 4a) exhibit a shift of the bands for V=O and V–O–V to higher wavenumbers with increased VO_x loading, which may be interpreted as resulting from oligomerization of surface vanadia species (6, 7, 14, 33). The DR-UV-vis spectra for these materials are generally consistent with this interpretation, supporting a gradual structural change from isolated $O{=}VO_3$ to an oligomeric species, which probably contains vanadium in a higher coordination number (Fig. 5a) (6, 7). Note that for samples calcined at 823 K, the same

transition from isolated VO_x to oligomeric species is observed by Raman and DR-UV-vis spectroscopy, but the earlier formation of ZrV_2O_7 at this temperature dominates the spectroscopic features for vanadium loadings of $\geq$14 wt%. The ^{51}V NMR spectra for samples calcined to 823 K also reveal this trend, with $5VO_x/ZrO_2$ containing predominantly pseudotetrahedral VO_x and $10VO_x/ZrO_2$ consisting mainly of a higher coordination number vanadium species. It is therefore apparent that increasing the vanadium loading or the calcination temperature have the similar effect of dramatically promoting the formation of ZrV_2O_7.

The surface areas of the uncalcined VO_x/ZrO_2 materials prepared by the thermolytic molecular precursor route (see Table 1) are as large as those previously observed for V/Zr/Si/O xerogels formed from $OV[OSi(O^tBu)_3]_3$ and $Zr[OCMe_2Et]_4$ (23), and they are much larger than those prepared by incipient wetness impregnation methods (180–340 $m^2\,g^{-1}$) (7). After calcination at 773 K under dry air, the VO_x/ZrO_2 materials described here have a larger surface area than materials with similar compositions but prepared by impregnation methods and calcined at 673 or 773 K (see Fig. 1) (7, 9). However, the observed surface areas are lower than those observed for V/Zr/Si/O materials calcined at 773 K, but this is probably due to the presence of silica in the latter (23). In general, we have observed that materials obtained by the thermolysis of alkoxides in nonpolar solvents exhibit high surface areas. We assume that this results from the lower capillary forces that develop during removal of the nonpolar solvent from pores in the material (21). For vanadia–zirconia materials calcined at 823 K, the surface areas are similar to those for materials prepared by impregnation methods and calcined at 773 K (7, 9).

For samples prepared by the wet impregnation method, the influence of vanadium loading on the surface area after calcination is much less pronounced than that for materials obtained by the thermolytic precursor route (7). In addition, reductions in surface area for the wet impregnation samples are observed above a V_2O_5 loading of 10 wt% (after calcination to 673 or 773 K), but the materials described here do not lose surface area until V_2O_5 loadings between 14 and 18% after calcination to 773 K (Fig. 1). Since the reductions in surface area with V_2O_5 content are believed to be related to the dispersion of VO_x on the zirconia surface (which affects the degree of sintering), it seems that the method described here may achieve a higher level of dispersion.

For analysis of intrinsic catalytic properties, it is often useful to derive activities and selectivities based on surface densities for the catalytically active species (6, 7, 47, 48). For VO_x/ZrO_2 catalysts prepared by the thermolytic molecular precursor method, this analysis is potentially complicated by the possibility that some of the vanadium is present in the bulk. Nonetheless, we can calculate apparent VO_x surface densities based on measured surface areas and the amount of added vanadium (Table 1), and on this basis the materials described here have a greater dispersion of VO_x than analogous materials formed by impregnation methods (due to the differences in surface areas at the same weight loadings of V_2O_5) (6, 7). As discussed above and below (based on catalyst performance), we believe that the VO_x species in these materials reside predominantly on the zirconia surface.

The crystallization behavior for materials obtained by the thermolytic molecular precursor route differs markedly from that observed for VO_x/ZrO_2 materials prepared by impregnation methods and calcined at the same temperature (6, 7). For the latter materials with a 2–30 wt% V_2O_5 loading (calcined to 773 K), *t*-ZrO_2 together with smaller amounts of *m*-ZrO_2 were observed in the X-ray diffraction patterns, and there was no evidence for ZrV_2O_7. Also, crystalline domains of V_2O_5 were observed by Raman spectroscopy at a 15 wt% loading (6, 7). For the alkoxide-derived materials calcined at the same temperature, Raman bands that might be assigned to trace amounts of V_2O_5 are not observed until the vanadia loading reaches 23 wt% (Fig. 4a). This comparison, and the greater extent to which ZrV_2O_7 is formed via the alkoxide method, also suggests that the molecular precursor route generates materials with a greater dispersion of vanadia (6, 7, 16). This idea is further supported by the greater inhibitions of *t*-ZrO_2 crystallization and the $t \rightarrow m$ ZrO_2 transformation that are observed for materials derived from the latter synthetic route (Fig. 2a).

Evaluation of the Catalysts

It is interesting to note that at similar vanadia surface densities the activities for VO_x/ZrO_2 materials calcined at 823 K are generally higher than those calcined at 773 K (Fig. 8, Tables 1–2). This may be ascribed to greater diffusion of vanadia to the zirconia surface at the higher calcination temperature.

Figure 9 provides activities and propene selectivities at a reaction temperature of 606 K as a function of VO_x surface density, for vanadia–zirconia materials prepared by either molecular precursor or impregnation methods, with subsequent calcination at 773 K (6, 7). The maximum rate of propane ODH for the material prepared from molecular precursors is greater than double the rate observed for the most active material obtained by impregnation. Note that the $10VO_x/ZrO_2$ sample calcined at 823 K is also about twice as active as the most active catalyst prepared by impregnation (Table 2). It is also interesting to note that the maximum rate of propene production is associated with an apparent surface density of 3–4 $VO_x\,nm^{-2}$, irrespective of the method of catalyst preparation. As mentioned earlier, this surface density corresponds approximately to the formation of oligomeric vanadium species.

The intrinsic propene selectivity of materials prepared from molecular precursors (extrapolated to zero

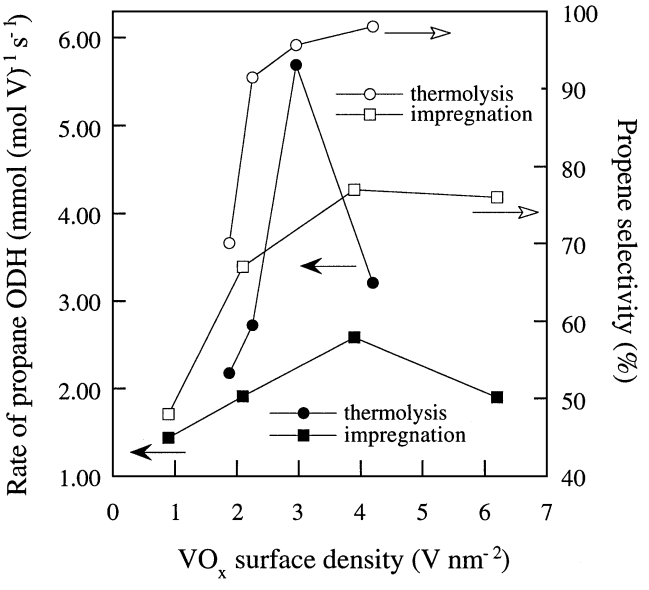

FIG. 9. Rate of propene production and propene selectivity as a function of apparent VO_x surface density for VO_x/ZrO_2 catalysts prepared by thermolysis and impregnation (6, 7) and subsequently calcined at 773 K. All reactions were carried out at 606 K with similar reactant ratios and pressures.

conversion of reactants) is markedly improved over that exhibited for materials prepared by impregnation (Fig. 9) (6, 7). The onset of a plateau of maximum selectivity occurs in both sets of samples, at a similar apparent surface density (3–4 VO_x nm^{-2}). At lower loadings of V_2O_5 (VO_x surface density <3 VO_x nm^{-2}), where an isolated VO_x species may predominate, the selectivity is lower (Figs. 8 and 9). This further supports the idea that oligomeric VO_x structures (as found in near-monolayer coverage) are more selective for propene production (6, 7).

Interestingly, the propene selectivity for the $23VO_x/ZrO_2$ material (calcined at 823 K) is relatively high (Table 3), even though the predominant vanadium-containing species in this sample is ZrV_2O_7. This result appears to conflict with an earlier assertion that bulk ZrV_2O_7 exhibits a propene selectivity of zero at 606 K (7). Currently it is not known why the results from the two studies are not in agreement, but this suggests that a more detailed investigation of ODH catalysis by ZrV_2O_7 may be worthwhile. This might be attributed to a greater dispersion of ZrV_2O_7 in materials prepared from the thermolysis of alkoxides, which leads to a greater number of readily assessible active sites.

In comparing VO_x/ZrO_2 catalysts prepared by different methods, and calcined to different temperatures, it is noteworthy that optimal catalytic properties (activity and selectivity) are achieved at similar V_2O_5 loadings (10–14 wt%) and apparent VO_x surface densities (3–4 VO_x nm^{-2}) (6, 7). This observation suggests that all samples contain active sites of the same type, and supports the view that the molecularly dispersed materials produced via the molecular precursor route segregate substantially upon calcination (*vida supra*). This segregation appears to continue as the catalysts derived from alkoxides are calcined to the higher temperature (823 K).

Given the comparisons described above, it follows that the observed differences in activities as a function of catalyst preparation method may be attributed to differences in the concentration of *catalytically active vanadium sites* produced by the two synthetic routes. Evidence for this difference is seen in Raman spectra, which reveal that samples prepared by impregnation exhibit bands for bulk V_2O_5 (which is known to exhibit low activity for the ODH of propane) at V_2O_5 loadings above 15 wt% (7). In contrast, catalysts prepared by the molecular precursor route do not contain observable bulk V_2O_5 until the V_2O_5 loading reaches 23 wt%. This difference is consistent with the fact that formation of V_2O_5 is known to be promoted under aqueous conditions (17, 18). Since the thermolytic molecular precursor method involves nonaqueous conditions, V_2O_5 does not form as readily. Therefore, we suggest that with the latter synthetic method, the nucleation and growth of VO_x species on the zirconia surface occur in a more controlled manner, under conditions that do not favor agglomeration of the vanadia into V_2O_5 particles, to give materials that have a greater dispersion of VO_x on zirconia. An alternative explanation is that samples prepared by thermolysis have a greater relative amount of oligomeric vanadium oxide and a lesser relative amount of isolated monovanadate species. This conclusion is supported by the observation that polyvanadate structures exhibit higher specific activity and selectivity for propene formation (6, 7, 33).

Previously it has been shown that propane reacts with oxygen in parallel and sequential steps over metal oxide catalysts (2, 4, 6, 7, 47, 48).

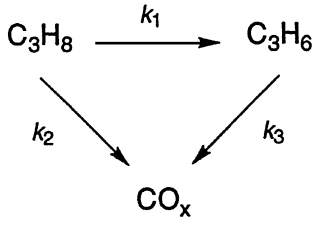

If oxygen consumption is low then pseudo-first-order rate coefficients for oxidative dehydrogenation (k_1), primary combustion of propane (k_2), and secondary combustion (k_3) of propene can be obtained from catalyst bed residence time data, and the details of this analysis have previously been derived and demonstrated (7).

Figure 10 shows that values of k_1 increase to a maximum and then decline with increasing apparent VO_x surface density for vanandia–zirconia materials prepared by both thermolysis and impregnation methods (calcined at

773 K), at a reaction temperature of 606 K. Both maxima are within a surface density of 3–4 VO_x nm^{-2}; however, the value of k_1 for the materials prepared from alkoxides is almost three times greater than that for catalysts prepared by impregnation. This is apparently due to the better dispersion of vanadia in the catalysts prepared from alkoxides, as mentioned above. The materials derived from molecular precursors and calcined at 823 K exhibit behavior that is identical to that of analogous materials calcined at 773 K.

The activation energies (E_{act}) of the vanadia–zirconia materials for the conversion of propane to propene were calculated from a plot of the logarithm of the intrinsic rate of propene production (ln k_1) with respect to $1/T$. For 5–23VO_x/ZrO_2 calcined at 773 K these ranged from 51–67 kJ mol^{-1} while those for the materials calcined at 823 K range from 62–73 kJ mol^{-1} (E_{act} for 10VO_x/ZrO_2 prepared by impregnation methods and calcined at 773 K was 99 kJ mol^{-1} (7, 47)).

A comparison of the k_2/k_1 ratio (obtained as described in Ref. 7)) for catalysts prepared by both impregnation and molecular precursor methods (calcined at 773 K) is presented in Fig. 11a. The materials prepared by impregnation approach a plateau of $k_2/k_1 = 0.3$ at a surface density of 3.7 VO_x nm^{-2} and higher (6, 7), while materials prepared by the thermolysis of alkoxides exhibit a plateau of $k_2/k_1 = 0.02$ at 4 VO_x nm^{-2}. This demonstrates that materials prepared by the thermolysis of alkoxides exhibit a lower relative activity for the combustion of propane.

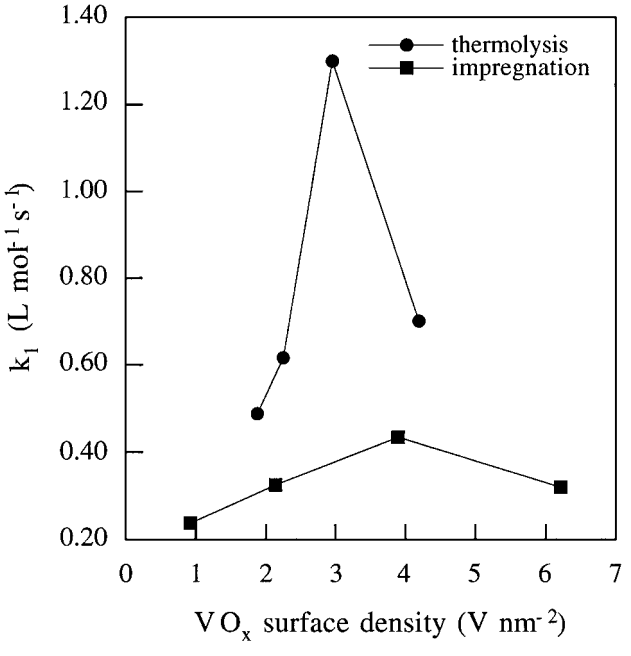

FIG. 10. Dependence of k_1 on apparent VO_x surface density for VO_x/ZrO_2 catalysts prepared by molecular precursor and impregnation (6, 7) methods and subsequently calcined at 773 K. All reactions were carried out at 606 K with similar reactant ratios and pressures.

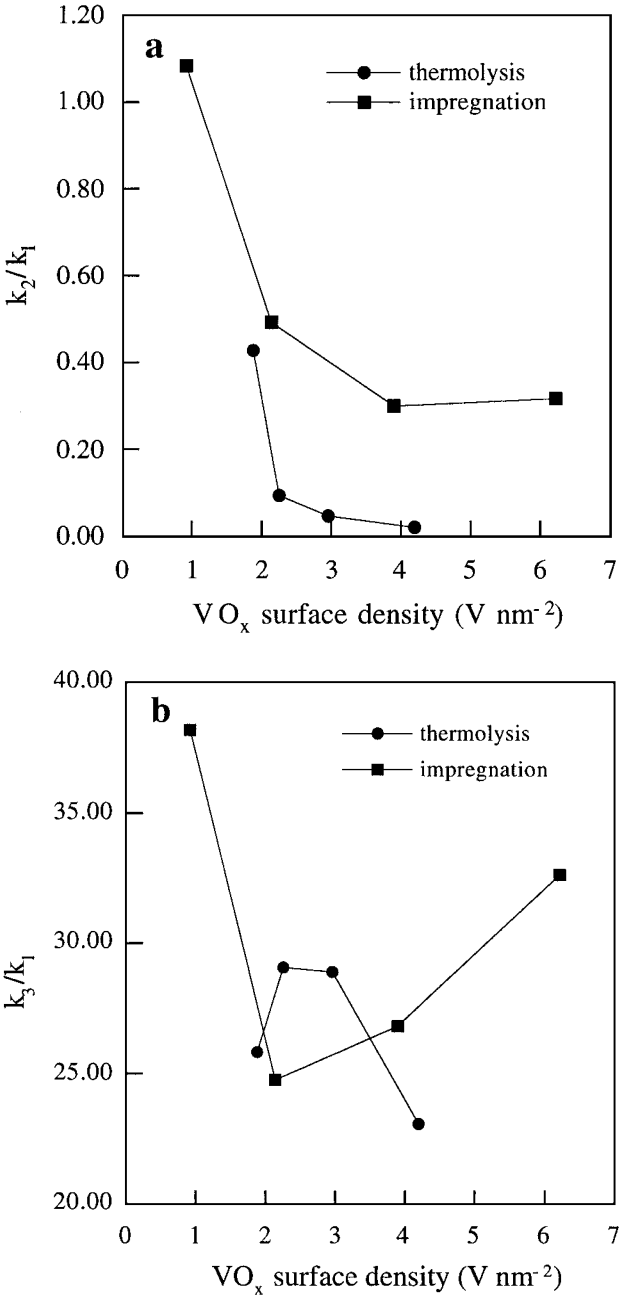

FIG. 11. Dependence of (a) k_2/k_1 and (b) k_3/k_1 on apparent VO_x surface density for VO_x/ZrO_2 catalysts prepared by molecular precursor and impregnation (6, 7) methods and subsequently calcined at 773 K. All reactions were carried out at 606 K with similar reactant ratios and pressures.

A plot of k_3/k_1 (derived as previously described in Ref. (7)) with respect to VO_x surface density is shown in Fig. 11b. It is seen that there is little difference between the k_3/k_1 ratios for samples prepared by either impregnation or thermolysis (calcined at 773 K). Since the values for k_1 are larger for materials prepared from the thermolysis of alkoxides (Fig. 10), it follows that the absolute values of k_3 must also be larger, and presumably the sites that

are more active for the conversion of propane to propene are also more active for the secondary combustion of propene.

CONCLUSIONS

The thermolytic decomposition of molecular precursors has been used to prepare a series of VO_x/ZrO_2 catalysts. The materials as produced upon thermolysis contain intimately mixed vanadium and zirconium oxides. Upon calcination, the zirconia segregates into a nanocrystalline phase, and vanadia spreads efficiently as VO_x species onto the surface of the nucleated zirconia. The resulting vanadia coating inhibits further crystallization for the zirconia nanoparticles, and phase transformations of zirconia. Under conditions that produce ZrV_2O_7, the catalytically active VO_x species are severely depleted, resulting in much lower catalytic activities.

The catalysts formed from the thermolytic molecular precursor route are superior to those obtained by conventional means in several respects. Significantly, this method produces materials with higher surface areas and better dispersions of the catalytically active VO_x species. Also, it appears to result in a more complete conversion of the vanadium species to catalytically active material. This active form of vanadia appears to feature oligomeric species with a vanadium coordination environment that is similar to that in V_2O_5, as indicated by spectroscopic investigations. Compared to catalysts prepared by the impregnation method, the catalysts described here are more active per vanadium for converting propane to propene, and more selective in that they exhibit lower rates for the direct combustion of propane to CO_x. However, it was also found that the alkoxide-derived catalysts are more active for the combustion of propene to CO_x. As a consequence, the ratio of secondary combustion to oxidative dehydrogenation (k_3/k_1) is similar for materials obtained by both methods. We are currently investigating the use of the thermolytic molecular precursor method in the synthesis of ODH catalysts with various compositions. This work should provide important information regarding the generality of the results described here.

ACKNOWLEDGMENTS

This work was supported by the Director, Office of Basic Energy Sciences, Chemical Sciences Division, of the U.S. Department of Energy under Contract DE-AC03-76SF00098. The authors acknowledge Enrique Iglesia for helpful discussions.

REFERENCES

1. *Chem. Eng. News* **77**, 19 (1999).
2. Albonetti, S., Cavani, F., and Trifirò, F., *Catal. Rev. Sci. Eng.* **38**, 413 (1996).
3. Mamedov, E. A., and Corberán, C. V., *Appl. Catal. A* **127**, 1 (1995).
4. Blasco, T., and López Nieto, J. M., *Appl. Catal. A* **157**, 117 (1997).
5. López Nieto, J. M., Soler, J., Concepción, P., Herguido, J., Menéndez, M., and Santamaría, J., *J. Catal.* **185**, 324 (1999).
6. Khodakov, A., Olthof, B., Bell, A. T., and Iglesia, E., *J. Catal.* **181**, 205 (1999).
7. Khodakov, A., Yang, J., Su, S., Iglesia, E., and Bell, A. T., *J. Catal.* **177**, 343 (1998).
8. Albrecht, S., Wendt, G., Lippold, G., Adamski, A., and Dyrek, K., *Solid State Ionics* **101–103**, 909 (1997).
9. Sohn, J. R., Cho, S. G., Pae, Y. I., and Hayashi, S., *J. Catal.* **159**, 170 (1996).
10. Chuah, G. K., *Catal. Today* **49**, 131 (1999).
11. Yang, J., M.Sc. Thesis, U.C. Berkeley (1998).
12. Deo, G., and Wachs, I. E., *J. Catal.* **146**, 323 (1994).
13. Huuhtanen, J., Sanati, M., Andersson, A., and Andersson, S. L. T., *Appl. Catal. A* **97**, 197 (1993).
14. Miyata, H., Kohno, M., Ono, Y., Ohno, T., and Hatayama, F., *J. Chem. Soc. Faraday Trans. 1* **85**, 3663 (1989).
15. Hatayama, F., Ohno, T., Yoshida, T., Ono, T., and Miyata, H., *React. Kinet. Catal. Lett.* **44**, 451 (1991).
16. Sanati, M., Andersson, A., Wallenberg, L. R., and Rebenstorf, B., *Appl. Catal A* **106**, 51 (1993).
17. Olthof, B., Khodakov, A., Bell, A. T., and Iglesia, E., *J. Phys. Chem. B* **104**, 1516 (2000).
18. van der Voort, P., White, M. G., Mitchell, M. B., Verberckmoes, A. A., and Vansant, E. F., *Spectrochim. Acta A* **53**, 2181 (1997).
19. Terry, K. W., Lugmair, C. G., Gantzel, P. K., and Tilley, T. D., *Chem. Mater.* **8**, 274 (1996).
20. Su, K., and Tilley, T. D., *Chem. Mater.* **9**, 588 (1997).
21. Terry, K. W., Lugmair, C. G., and Tilley, T. D., *J. Am. Chem. Soc.* **119**, 9745 (1997).
22. Terry, K. W., and Tilley, T. D., *Chem. Mater.* **3**, 1001 (1991).
23. Rulkens, R., and Tilley, T. D., *J. Am. Chem. Soc.* **120**, 9959 (1998).
24. Rulkens, R., Male, J. L., Terry, K. W., Olthof, B., Khodakov, A., Bell, A. T., Iglesia, E., and Tilley, T. D., *Chem. Mater.* **11**, 2966 (1999).
25. Su, K., Tilley, T. D., and Sailor, M. J., *J. Am. Chem. Soc.* **118**, 3459 (1996).
26. Lugmair, C. G., Tilley, T. D., and Rheingold, A. L., *Chem. Mater.* **11**, 1615 (1999).
27. Coles, M. P., Lugmair, C. G., Terry, K. W., and Tilley, T. D., *Chem. Mater.* **12**, 122 (2000).
28. Sing, K. S. W., Everett, D. H., Haul, R. A. W., Moscou, L., Pierotti, R. A., Rouquérol, J., and Siemieniewska, T., *Pure Appl. Chem.* **57**, 603 (1985).
29. Zhan, Z., and Zeng, H. C., *J. Mater. Res.* **13**, 2174 (1998).
30. Klug, H. P., and Alexander, L. E., "X-Ray Diffraction Procedures—For Polycrystalline and Amorphous Materials." Wiley–Interscience, New York, 1974.
31. Su, S. C., and Bell, A. T., *J. Phys. Chem. B* **102**, 7000 (1998).
32. Anastasskis, E., Papanicolaou, B., and Asher, I. M., *J. Phys. Chem. Solids* **36**, 667 (1975).
33. Prinetto, F., Ghiotti, G., Occhiuzzi, M., and Indovina, V., *J. Phys. Chem. B* **102**, 10316 (1998).
34. Kornatowski, J., Wichterlová, B., Jirkovsky, J., Löffler, E., and Pilz, W., *J. Chem. Soc. Faraday Trans.* **92**, 1067 (1996).
35. Amado, A. M., Aureliano, M., Ribeiro-Claro, P. J. A., and Teixeira-Dias, J. J. C., *J. Raman Spectrosc.* **24**, 699 (1993).
36. Deo, G., and Wachs, I. E., *J. Phys. Chem.* **95**, 5889 (1991).
37. Roozeboom, F., Mittelmeijer-Hazeleger, M. C., Moulijn, J. A., de Beer, V. H. J., and Gellings, P. J., *J. Phys. Chem.* **84**, 2783 (1980).
38. Khoarovani, N., Sleight, A. W., and Vogt, T., *J. Solid State Chem.* **132**, 355 (1997).

39. Curran, M. D., Gedris, T. E., Stiegman, A. E., and Plett, G. A., *Chem. Mater.* **11**, 1120 (1999).
40. Das, N., Eckert, H., Hu, H., Wachs, I. E., Walzer, J. F., and Feher, F. J., *J. Phys. Chem.* **97**, 8240 (1993).
41. Eckert, H., and Wachs, I. E., *J. Phys. Chem.* **93**, 6796 (1989).
42. Barton, D. G., Soled, S. L., Meitzner, G. D., Fuentes, G. A., and Iglesia, E., *J. Catal.* **181**, 57 (1999).
43. Adamski, A., Sojka, Z., Dyrek, K., and Che, M., *Solid State Ionics* **117**, 113 (1999).
44. Mitsuhashi, T., Ichihara, M., and Tatsuke, U., *J. Am. Ceram. Soc.* **57**, 97 (1974).
45. Heuer, A. H., Claussen, N., Kriven, W. M., and Rühle, M., *J. Am. Ceram. Soc.* **65**, 642 (1982).
46. Nagarajan, V. S., and Rao, K. J., *J. Mater. Sci.* **24**, 2140 (1989).
47. Chen, K., Bell, A. T., and Iglesia, E., *J. Phys. Chem. B* **104**, 1292 (2000).
48. Chen, K., Khodakov, A., Yang, J., Bell, A. T., and Iglesia, E., *J. Catal.* **186**, 325 (1999).